

Multi-soliton states under triangular spatial modulation of the quadratic nonlinearity

Vitaly Lutsky¹ and Boris A. Malomed^{1,2}

¹Department of Physical Electronics, School of Electrical Engineering,
Tel Aviv University, Tel Aviv 69978, Israel

²ITMO University, St. Petersburg 197101, Russia

March 2, 2022

Abstract

We introduce multi-soliton sets in the two-dimensional medium with the $\chi^{(2)}$ nonlinearity subject to spatial modulation in the form of a triangle of singular peaks. Various families of symmetric and asymmetric sets are constructed, and their stability is investigated. Stable symmetric patterns may be built of 1, 4, or 7 individual solitons, while stable asymmetric ones contain 1, 2, or 3 solitons. Symmetric and asymmetric patterns may demonstrate mutual bistability. The shift of the asymmetric single-soliton state from the central position is accurately predicted analytically. Vortex rings composed of three solitons are produced too.

1 Introduction

The significance of solitons (self-trapped modes) in various areas of physics is commonly known [1, 2]. Recently, considerable attention has been drawn to possibilities to extend the variety of solitons in nonlinear media by imposing spatial modulation on the local strength of the nonlinear interaction, i.e., the creation of effective nonlinear potentials for solitons (alias *pseudopotentials*, as they were originally called in solid-state physics [3]). Many results produced in this direction were collected in review [4]. A majority of studies performed in this area dealt with the ubiquitous cubic, alias $\chi^{(3)}$, nonlinearity, which finds commonly known realizations in optics, in the form of self-focusing of optical beams due to the Kerr effect [1], and as collisional interactions in atomic Bose-Einstein condensates (BECs) [5]. In optical media, spatial modulation of the local Kerr coefficient can be induced by means of inhomogeneous distributions of resonant dopants, which enhance the $\chi^{(3)}$ nonlinearity via two-photon resonance [6]. In BEC, a similar effect can be produced by means of inhomogeneous optical [7, 8] or magnetic [9] fields, as well as a combination of both [10], which affect the local strengths of the collisional nonlinearity via the Feshbach resonance.

A specific ramification of such models in one dimension (1D) is based on a locally singular modulation of the self-focusing in the form of a cusp, with coefficient $\chi^{(3)} \sim |x|^{-\alpha}$, which was introduced in Ref. [11]. The relevant range of values of the singular-modulation power is $0 \leq \alpha < 1$. This model offers a

possibility to generalize the study of the onset of collapse in nonlinear media [12, 13], as well as to emulate the nonlinear dynamics in a sub-1D space, with the effective dimension $D = 2(1 - \alpha)/(2 - \alpha) < 1$ [11]. The singular modulation can be emulated by means of above-mentioned techniques, tuning them to the exact resonance in a narrow layer.

Another possibility is to consider spatial modulation of the local interaction strength in media with the quadratic ($\chi^{(2)}$) nonlinearity, which has well-known realizations in optics [14]-[17]. Experimental realizations of such settings are possible, in particular, using the well-elaborated technique of the quasi-phase-matching [18]-[20], which can be implemented in a spatially nonuniform form, in 1D and 2D geometries alike, thus helping one to create a required profile of the $\chi^{(2)}$ coefficient [21]-[23]. In the theoretical analysis, singular modulation of the quadratic nonlinearity in the 1D system, accounted for by a delta-function, $\chi^{(2)}(x) \sim \delta(x)$, and localized modes (solitons) pinned to it, were introduced in Ref. [24], and a pair of modulating delta-functions was considered in Ref. [25]. A discrete version of the localized quadratic nonlinearity was elaborated in the form of a linear lattice with one or two $\chi^{(2)}$ -nonlinear sites embedded in it [26].

While the delta-like modulation of the local $\chi^{(2)}$ coefficient may not be easily realized in the experiment, a more realistic case of the 1D singular modulation, with $\chi^{(2)} \sim |x|^{-\alpha}$ and positive α , was introduced in Ref. [27]. It was found that this modulation format supports quadratic solitons, pinned to the singular peak, for $\alpha < 1$ (the pinned modes vanish at $\alpha = 1$), and they are chiefly stable. A natural extension of that setting is a symmetric pair of two peaks (similar to the above-mentioned symmetric set of two delta-functions multiplying the nonlinear terms [25]). The consideration of the twin peaks has made it possible to predict effects of the spontaneously symmetry breaking [28] and formation of asymmetric two-soliton states pinned to the two peaks [27]. These results may be used for the design of steering optical beams in the form of spatial solitons.

An essential advantage of using the quadratic nonlinearity with this type of the local modulation is that it may be extended to the 2D geometry, by choosing $\chi^{(2)}(r) \sim r^{-\alpha}$ (r is the radial coordinate), while any 2D singular modulation of the self-focusing $\chi^{(3)}$ nonlinearity leads to collapse. In terms of optics, the 2D system models light propagation in bulk media with the quadratic nonlinearity. In particular, the model admits stable spatial solitons, which represent self-trapped light beams in the bulk medium [14]-[16]. The analysis of the 2D setting, performed in Ref. [27], has revealed that the solitons, pinned to the singular-modulation peak, exist at $\alpha < 2$, and they have a stability region at $\alpha < 0.5$. Solitons with embedded vorticity can also be pinned to the singularity peak, but they all are unstable.

The availability of stable 2D solitons attached to the singular-modulation peak suggests a possibility to study multi-soliton patterns in multi-peak modulation profiles, subject to natural symmetry conditions. The simplest profile which realizes the 2D symmetry is an equilateral set of three peaks, cf. Refs. [29]-[34]. This is the subject of the present paper, which is structured as follows. The model is introduced in Section II. In Section III, we report numerical results for the existence and stability of various patterns, which may be classified as symmetric and asymmetric ones, with respect to the underlying triangular modulation structure. Some results are also obtained in an analytical form, *viz.*, prediction of an asymmetric location of a single soliton between the three singular cusps. Section IV deals with ring-shaped three-soliton sets which carry

the phase circulation of 2π , i.e., composite vortices admitted by the three-peak modulation structure, cf. Refs. [35]-[38]. The paper is concluded by Section V.

2 The model

Dynamical models for self-guided beams in $\chi^{(2)}$ media have been studied in detail, as summarized in reviews [14]-[17]. In the present work, we focus on the basic case of the two-wave (degenerate, alias Type-I) quadratic interactions in the bulk medium, which are modeled by the system of 2D spatial-domain equations for complex amplitudes of the fundamental-frequency (FF) and second-harmonic (SH) waves, $u(x, y, z)$ and $v(x, y, z)$. Here, following the above-mentioned direction of studies of the nonlinear wave propagation in media with a locally modulated nonlinearity strength [4], we consider the system with an (x, y) -dependent $\chi^{(2)}$ coefficient. As also said above, the case of singular modulation is an especially interesting one. Thus, the 2D system with the cusp-shaped modulation of the $\chi^{(2)}$ coefficient is written, in the scaled form, as

$$iu_z + \frac{1}{2}\nabla^2 u + r^{-\alpha}u^*v = 0, \quad (1)$$

$$2iv_z + \frac{1}{2}\nabla^2 v - Qv + \frac{1}{2}r^{-\alpha}u^2 = 0, \quad (2)$$

where z is the propagation distance, diffraction operator $(1/2)\nabla^2$ acts on transverse coordinates (x, y) , $r \equiv \sqrt{x^2 + y^2}$, the asterisk stands for the complex conjugate, and real coefficient Q represents the SH-FF mismatch. By means of obvious rescaling, we fix the mismatch parameter to take one of three values,

$$Q = 0, +1, -1. \quad (3)$$

In fact, similar results are obtained for all the three values defined in Eq. (3).

Localized solutions of Eqs. (1) and (2) are characterized by the total power (alias the Manley-Rowe invariant),

$$P = \int \int [|u(x, y)|^2 + 4|v(x, y)|^2] dx dy, \quad (4)$$

which is a dynamical invariant of the system, along with its Hamiltonian,

$$H = \int \int \left\{ \frac{1}{2} (|\nabla u|^2 + |\nabla v|^2) - \frac{1}{2} r^{-\alpha} [u^2 v^* + (u^*)^2 v] + Q|v|^2 \right\} dx dy. \quad (5)$$

The isotropic configuration with the single-peak modulation conserves the angular momentum too. However, the triangular setting considered below is anisotropic, breaking the angular-momentum conservation.

Positive exponent α in Eqs. (1) and (2) determines the form of the singularity, $\alpha = 0$ corresponding to the uniform medium. As mentioned above, a basic result reported in Ref. [27] is that these equations generate fundamental (zero-vorticity) localized states pinned to the singular-modulation peak at $\alpha < 2$, and these states have a stability area at $\alpha < 0.5$. Under this condition, they tend to be stable and unstable, respectively, at smaller and larger values of the total power, P , at all values of the mismatch, see Eq. (3).

Stationary solutions to Eqs. (1), (2) with real propagation constant k are looked for as

$$\{u(x, y, z), v(x, y, z)\} = \{e^{ikz}\varphi(x, y), e^{2ikz}\psi(x, y)\}, \quad (6)$$

with functions $\varphi(x, y)$ and $\psi(x, y)$ (which are complex for vortex modes) obeying the stationary equations:

$$-k\varphi + \frac{1}{2}\nabla^2\varphi + r^{-\alpha}\varphi^*\psi = 0, \quad (7)$$

$$-4k\psi + \frac{1}{2}\nabla^2\psi - Q\psi + \frac{1}{2}r^{-\alpha}\varphi^2 = 0. \quad (8)$$

The dependence between the total power and k , obtained in a numerical form from Eqs. (7) and (8), satisfies the Vakhitov-Kolokolov criterion, $dP/dk > 0$ (for all values of mismatch, Q), which is a well-known necessary, but not sufficient, stability criterion for solitons [42, 12, 13].

Solutions to Eqs. (7) and (8) may also be looked for as vortices with integer topological charge m in its FF components (and charge $2m$ in the SH component) [43, 44], i.e.,

$$\varphi = e^{im\theta}U(r), \psi = e^{2im\theta}V(r), \quad (9)$$

in terms of the polar coordinates (r, θ) , with real radial functions U and V obeying the following equations:

$$-kU + \frac{1}{2}\left(\frac{d^2}{dr^2} + \frac{1}{r}\frac{d}{dr} - \frac{m^2}{r^2}\right)U + r^{-\alpha}VU = 0, \quad (10)$$

$$-4kV + \frac{1}{2}\left(\frac{d^2}{dr^2} + \frac{1}{r}\frac{d}{dr} - \frac{m^2}{r^2}\right)V - QV + \frac{1}{2}r^{-\alpha}U^2 = 0, \quad (11)$$

supplemented by boundary conditions $U \sim r^{|m|}$ and $V \sim r^{2|m|}$ at $r \rightarrow 0$. Unlike the fundamental modes, all the vortical ones supported by the single peak were found to be unstable [27], similar to the well-known instability of 2D solitons with embedded vorticity in the uniform $\chi^{(2)}$ medium [43]-[46].

The subject of the consideration in the present work is the set of three equally separated singular-modulation peaks, which is represented by the following ‘‘triangular’’ modulation profile, labeled by symbol Δ :

$$\chi_{\Delta}^{(2)}(\alpha, X_{A,B,C}, Y_{A,B,C}) = [(x - X_A)^2 + (y - Y_A)^2]^{-\frac{\alpha}{2}} + [(x - X_B)^2 + (y - Y_B)^2]^{-\frac{\alpha}{2}} + [(x - X_C)^2 + (y - Y_C)^2]^{-\frac{\alpha}{2}}. \quad (12)$$

Here $(X_{A,B,C}, Y_{A,B,C})$ are coordinates of the three peaks, each located at distance R from the center, as shown in Fig.(1). The respective system of the coupled FF-SH propagation equations is written as

$$iu_z + \frac{1}{2}\nabla^2u + \chi_{\Delta}^{(2)}(\alpha, X_{A,B,C}, Y_{A,B,C})u^*v = 0, \quad (13)$$

$$iv_z + \frac{1}{2}\nabla^2v - Qv + \frac{1}{2}\chi_{\Delta}^{(2)}(\alpha, X_{A,B,C}, Y_{A,B,C})u^2 = 0. \quad (14)$$

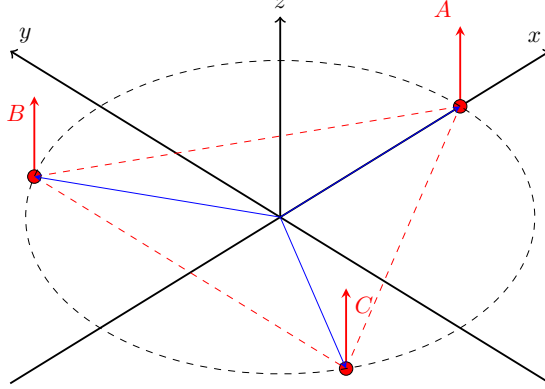


Figure 1: The set of three singularity peaks A, B, and C of the nonlinearity modulation, each one separated by distance R from the center.

The stationary version of Eqs. (13) and (14) is

$$-k\varphi + \frac{1}{2}\nabla^2\varphi + \chi_{\Delta}^{(2)}(\alpha, X_{A,B,C}, Y_{A,B,C})\varphi^*\psi = 0, \quad (15)$$

$$-4k\psi + \frac{1}{2}\nabla^2\psi - Q\psi + \frac{1}{2}\chi_{\Delta}^{(2)}(\alpha, X_{A,B,C}, Y_{A,B,C})\varphi^2 = 0, \quad (16)$$

cf. Eqs. (7) and (8). Solutions to Eqs. (15) and (16) were produced by means of two numerical schemes, *viz.*, the Newton's conjugate gradient method, and the squared operator method [39], which are appropriate techniques in this context. In particular, the Newton's algorithm provides convergence of the numerical solutions after fewer iterations than demanded by other numerical schemes.

The stability analysis for stationary states was performed by taking perturbed solutions in the usual form [39, 40],

$$u = [\varphi(x, y) + \epsilon_u(x, y, z)] e^{ikz}, \quad (17)$$

$$v = [\psi(x, y) + \epsilon_v(x, y, z)] e^{2ikz}, \quad (18)$$

with perturbation eigenmodes looked for as

$$\begin{cases} \epsilon_u = \xi_u^+(x, y)e^{\lambda z} + \xi_u^-(x, y)e^{-\lambda^* z}, \\ \epsilon_v = \xi_v^+(x, y)e^{\lambda z} + \xi_v^-(x, y)e^{-\lambda^* z}, \end{cases} \quad (19)$$

where λ is the respective eigenvalue (that may be complex), instability corresponding to $\text{Re}(\lambda) \neq 0$. The corresponding eigenvalue problem for the linearized equations was then solved by means of the spectral collocation method [39]. Finally, the so predicted stability was checked in direct simulations of the evolution of perturbed solutions of Eqs. (15) and (16). The simulations were run by means of the fourth-order Runge-Kutta algorithm, implemented in the 2D Cartesian coordinates.

3 Numerical results: Zero-vorticity patterns

3.1 The fundamental mode pinned to the single peak

Zero-vorticity (alias fundamental) states were found as numerical solutions of Eqs. (15) and (16), with the help of the above-mentioned Newton's and conjugate-gradient method, following the pattern presented in book [39]. Before proceeding to the consideration of the triangular scheme, it was necessary to create appropriate building blocks, in the form of solutions pinned to the single modulation peak, i.e., solutions in the form of expressions (9), with the radial functions satisfying Eqs. (10) and (11). The latter equations were solved starting from the input in the form of

$$U(r) = Ar^m \exp(-\rho r^2), V(r) = Br^{2m} \exp(-\gamma r^2), \quad (20)$$

with constants A , B and $\rho > 0$, $\gamma > 0$.

Note that the same expressions (20) can be used as the ansatz for constructing the VA (variational approximation), using the Lagrangian of Eqs. (10) and (11),

$$L = \int_0^\infty r dr \left\{ \frac{1}{2} \left[\left(\frac{dU}{dr} \right)^2 + \left(\frac{dV}{dr} \right)^2 \right] + \left[\left(k + \frac{m^2}{2r^2} \right) U^2 + \left(4k + \frac{2m^2}{r^2} + Q \right) V^2 - r^{-\alpha} U^2 V \right] \right\}. \quad (21)$$

The substitution of *ansatz* (20) in the Lagrangian yields the following effective Lagrangian:

$$L = \frac{1}{2} \left\{ 4^{-m} B^2 m (4k + Q) \gamma^{-1-2m} \Gamma(2m) + \frac{1}{2} 4^{-m} B^2 \gamma^{-2m} \Gamma(2 + 2m) \right\} + \frac{1}{4} A^2 \left\{ 2^{-m} \rho^{-1-m} [k \Gamma(1 + m) + \rho \Gamma(2 + m)] - 2B(\gamma + 2\rho)^{-1-2m+\frac{\alpha}{2}} \Gamma\left(1 + 2m - \frac{\alpha}{2}\right) \right\}, \quad (22)$$

where Γ is the Euler's Gamma-function. In the framework of the VA, amplitudes A , B and inverse square widths of the two components, ρ and γ , were found, for given k and m , from the Euler-Lagrange equations, $\partial L / \partial B = \partial L / \partial (A^2) = \partial L / \partial \rho = \partial L / \partial \gamma = 0$, applied to Lagrangian (22). This system of algebraic equations was solved numerically.

The practical significance of the VA is in the fact that it predicts the mode pinned to an individual peak in the explicit analytical form (20). Then, appropriate superpositions of such modes, with separated centers, can be immediately used as inputs for generating multi-mode patterns pinned to the set of three peaks. This approach works efficiently even in cases when the accuracy of the VA-predicted mode for the single peak is relatively poor, in comparison with the corresponding full numerical solution.

3.2 Symmetric fundamental modes in the three-peak configuration

The numerical solution of Eqs. (15) and (16) reveals many species of stationary patterns pinned to the three-peak modulation profiles, both stable and unstable ones. Some stationary states share the three-fold symmetry of the underlying triangular profile. They were found to be stable in three cases:

- Single-soliton states, placed at the midpoint (central position) between the three peaks. Their shape is very similar to the well-known stable 2D fundamental solitons in uniform $\chi^{(2)}$ media [15, 16], see an example in Fig. 2.
- Four-soliton sets, composed of three identical solitons placed close to the three modulation peaks, and an additional soliton, with the sign of its FF component opposite to that of the other three constituents of the set, which is placed at the midpoint (the sign of the SH component is the same for all the four solitons, and their local peak powers, i.e., maximum values of $|\varphi(x, y)|^2$ and $|\psi(x, y)|^2$, are nearly equal too). The opposite signs of the FF components make the interaction between the central soliton and ones belonging to the surrounding triad repulsive [47], which is compensated by attraction of the latter solitons to neighboring singularities of nonlinearity strength. An example of a stable four-soliton patterns in displayed in Fig. 3.
- Seven-soliton sets, composed, as above, of three identical solitons placed very close to the three modulation peaks, an additional soliton, placed at the midpoint, and three other ones, which are located on the extension of lines connecting the midpoint with each peak, see an example in Fig. 4. In this case too, the sign of the FF component of the four additional solitons is opposite to that of the triad directly pinned to the singular-modulation peaks, while the signs of the SH component are the same for all the seven constituents, and their peak powers are nearly equal.

More complex symmetric patterns were found too, including a 10-soliton set shown in Fig. (5). However, all the symmetric sets constructed of more than seven solitons were found to be unstable. In direct simulations, unstable multi-soliton complexes spontaneously transform themselves into simpler stable ones – see, for instance, the transformation of an unstable seven-soliton set into a stable two-soliton one in Fig. 6.

3.3 Asymmetric fundamental modes

The same three-peak modulation profile may also support soliton sets which break the triangular symmetry. The simplest among them are asymmetric stationary single-soliton states, which are shifted from the central position along the line connecting the center of the three-peak structure and one of the peaks, in the direction opposite to that towards the peak (see Fig. 8(a)). It is possible to predict the shift analytically, making use of the $\chi^{(2)}$ term in Hamiltonian H (5). Indeed, assuming that the soliton has a size much smaller than its distance

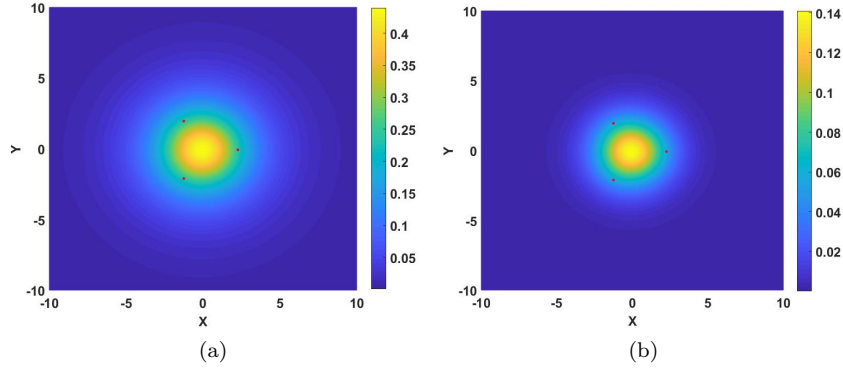


Figure 2: (Color online) A stable symmetric single-soliton pattern, with the following values of parameters in Eqs. (12)-(16): the modulation-singularity power $\alpha = 0.15$, mismatch $Q = +1$, and distance of each singularity peak from the center $R = 2.3438$ (here and in similar plots displayed below, red dots show location of the singularities). The propagation constant corresponding to this soliton set is $k = 0.1$. Panels (a) and (b) display the stationary FH and SH fields, $\varphi(x, y)$ and $\psi(x, y)$, respectively.

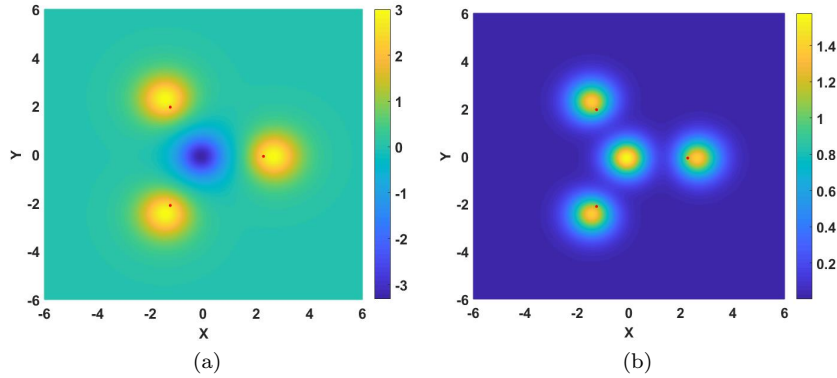


Figure 3: (Color online) A stable set of four solitons, with parameters $\alpha = 0.15$, $Q = +1$, and $R = 2.3438$. The propagation constant corresponding to this soliton set is $k = 1.1$. Panels (a) and (b) display the FH and SH fields, $\varphi(x, y)$ and $\psi(x, y)$, respectively.

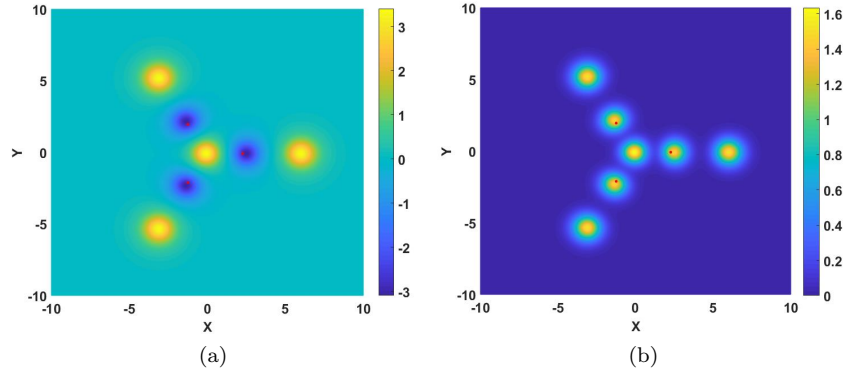


Figure 4: (Color online) The same as in Fig. 3, but for a stable set of seven solitons, with parameters $\alpha = 0.15$, $Q = 1$, $R = 2.3438$, and $k = 1.1$.

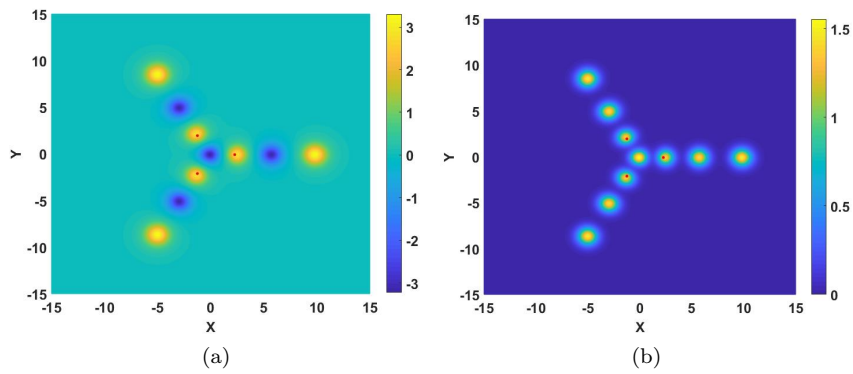


Figure 5: (Color online) The same as in Figs. 3 and 4, but for an unstable symmetric set of ten solitons, with parameters $\alpha = 0.15$, $Q = 1$, $k = 1$, and $R = 2.3438$.

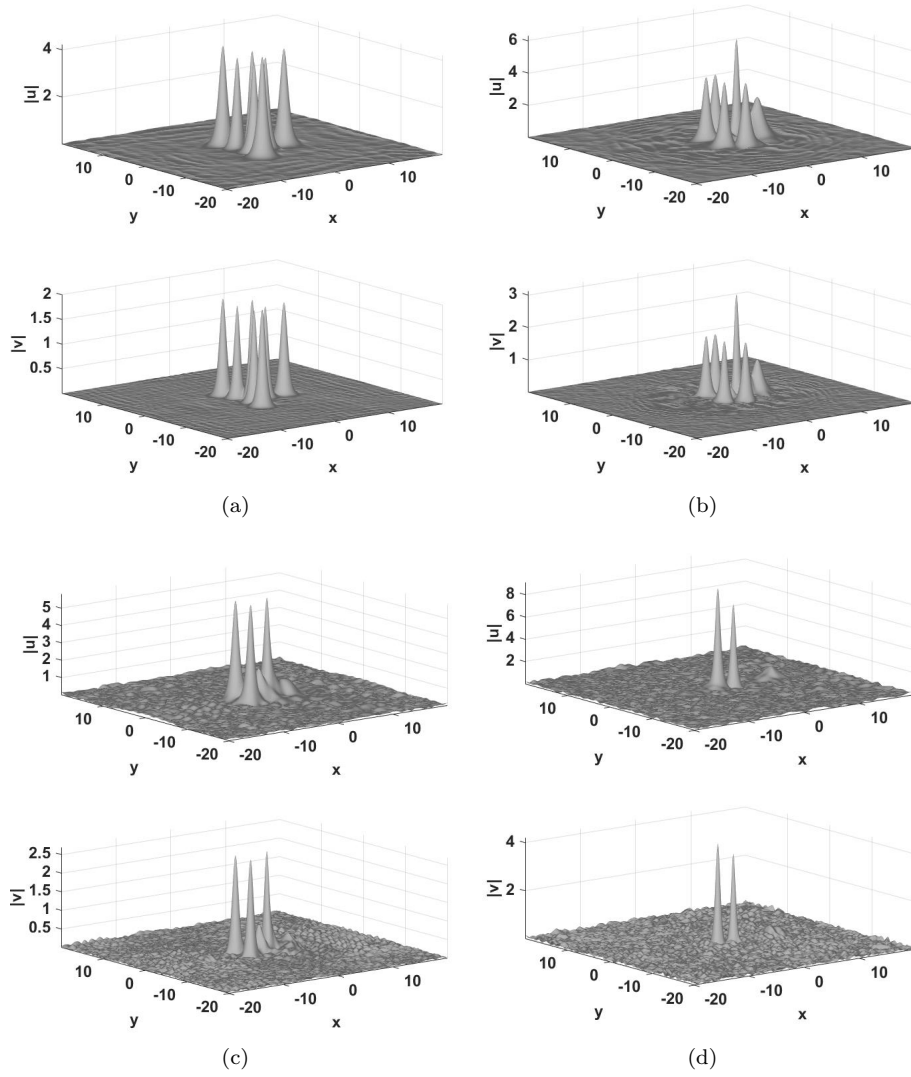


Figure 6: Instability-induced spontaneous transformation of a set of seven solitons into a stable two-soliton state, for parameters $Q = 1$, $\alpha = 0.15$, $R = 2.3438$, and the propagation constant of the initial configuration $k = 1.1$. Panels (a), (b), (c) and (d) display, respectively, shapes of the absolute values of the FF and SH fields at $z = 20, 60, 80$ and 100 .

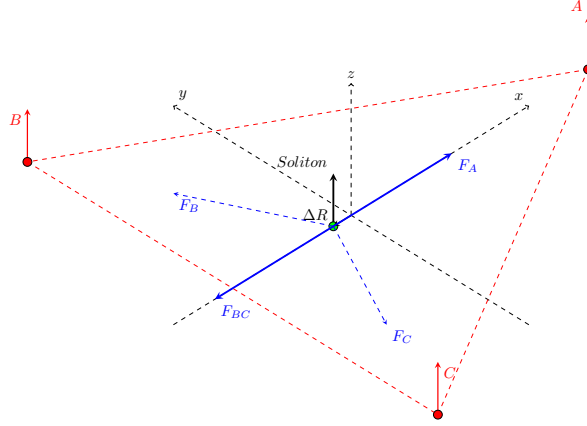


Figure 7: (Color online) The force-equilibrium diagram for the soliton shifted from the midpoint by distance ΔR , see details in the text.

$\rho \approx R$ from the singular-modulation peak, the energy of the soliton's attraction to a particular peak can be written as

$$E_{\text{attr}} \approx -E_0 \rho^{-\alpha}, \quad E_0 = \iint \text{Re} \{ \varphi^2(x, y) \psi(x, y) \} dx dy, \quad (23)$$

where ρ is the distance of the soliton's center from the peak, and $\varphi(x, y)$ and $\psi(x, y)$ are components of stationary solution (6) for the soliton. In fact, it may be taken as the standard solution for the 2D soliton in the uniform medium [15, 16], with quadratic coefficient $\chi^{(2)} = 3R^{-\alpha}$, as per Eq. (12). The corresponding attraction force is

$$F = -\partial E_{\text{attr}} / \partial \rho = -E_0 \rho^{-(1+\alpha)}. \quad (24)$$

Then, a possible equilibrium position of the soliton, treated as a quasi-particle shifted from the center by distance ΔR , along the axis connecting the central point and the peak, which corresponds to $\rho = R + \Delta R$, can be predicted by the condition of the balance between forces F_A and F_B, F_C attracting the soliton to the three peaks, as shown in Fig. 7. An elementary consideration gives rise to the balance condition in the following form:

$$(1 + \delta)^{-(1+\alpha)} = (1 - 2\delta) \left(\frac{3}{4} + \left(\frac{1}{2} - \delta \right)^2 \right)^{-(1+\alpha/2)}, \quad (25)$$

where $\delta \equiv (\Delta R)/R$, the right-hand side in Eq. (25) being produced by the projection of the forces of the attraction to two other peaks onto the axis connecting the midpoint and the first peak, see Fig. 7. Assuming $\alpha \ll 1$ (which approximately holds for values considered here, such as $\alpha = 0.15$), an expansion of Eq. (25) in powers of small α and presumably small δ yields a simple lowest-order result for the asymmetric equilibrium position of the soliton: $\delta = \alpha/2$. In particular, for $\alpha = 0.15$ this result is $\delta = 0.075$, while a numerical solution

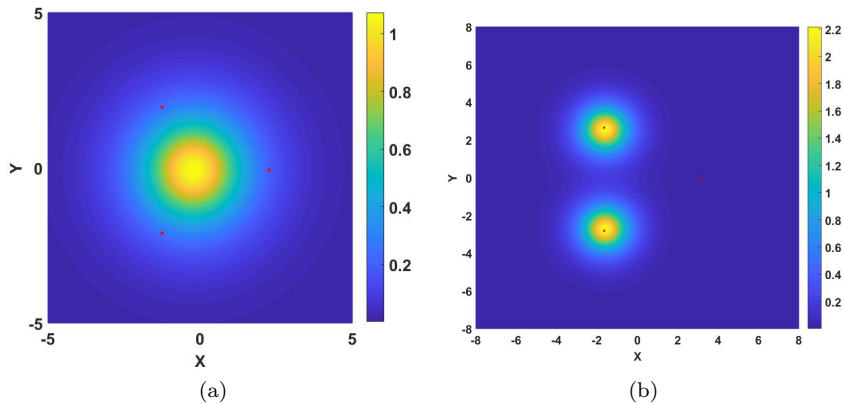


Figure 8: (Color online) (a) The FH field of a stable asymmetric single-soliton state, whose stationary position is shifted off the center. The parameters are $\alpha = 0.15$, $Q = 1$, and $R = 2.3438$, the respective propagation constant being $k = 0.35$ (b) The same for a stable asymmetric two-soliton set, with $\alpha = 0.15$, $Q = 1$, $R = 3.1250$, and $k = 1.1$.

of Eq. (25) for the same $\alpha = 0.15$ gives $\delta = 0.068$. The full numerical solution for the single asymmetrically placed soliton, displayed in Fig. 8(a), yields $\delta_{\text{num}} = 0.069$, which corroborates the analytical prediction quite well.

An additional straightforward consideration demonstrates that the so predicted equilibrium position is a local minimum of the potential corresponding to forces given by Eq. (24), i.e., this position is stable, which is corroborated by the numerical results. In this connection, it is relevant to mention that the obvious central equilibrium position, at $\delta = 0$, which represents the symmetric single-soliton state, corresponds to a local maximum of the same potential, hence it is formally unstable, while in the numerical simulations these states are stable (see Fig. 10(a) below). However, in reality all stable symmetric single-soliton modes exist with small values of k in Fig. 10(a), hence they are quite broad, covering nearly the entire triangle formed by the three singular-modulation peaks, as clearly seen in Fig. 2; for this reason, the above treatment of the soliton as a quasi-particle is not relevant in this case. On the other hand, values of k for stable asymmetric single-soliton states in Fig. 10(a) are larger than for their symmetric counterparts, making these solitons more compact objects (as corroborated by Fig. 8(a)), for which the quasi-particle approximation is appropriate.

Stable two-soliton asymmetric sets were found too, for relatively large values of R , with two singularity peaks carrying solitons pinned to them, while the third one remains nearly “empty”, see Fig. 8(b). The largest number of individual solitons in stable asymmetric patterns is three (unlike seven for the symmetric sets). Larger asymmetric complexes were found too, such as a slightly bent five-soliton string shown in Fig. (9), but they all are unstable. Note that, similar to the symmetric multi-soliton sets, adjacent solitons in the string have opposite signs in their FF components.

Results obtained for the existence and stability of various single- and multi-soliton complexes are summarized in Fig. (10), in the form of $P(k)$ dependences

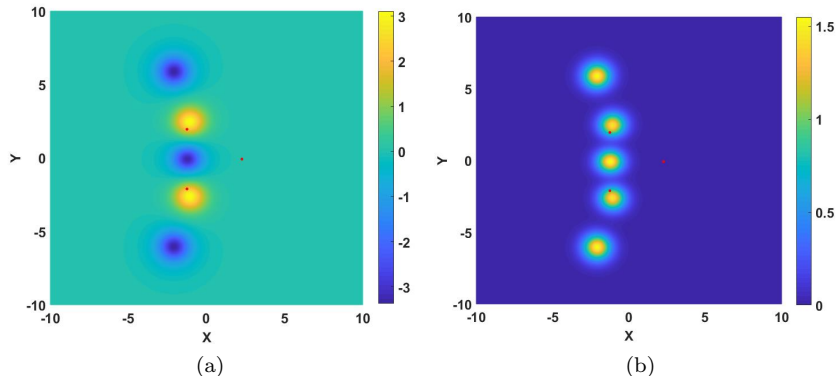


Figure 9: (Color online) An unstable asymmetric set of five solitons, for parameters $\alpha = 0.15$, $Q = 1$, and $R = 2.3438$, the propagation constant being $k = 1.1$. Panels (a) and (b) display the FH and SH fields, $\varphi(x, y)$ and $\psi(x, y)$, respectively.

for different species of the multisoliton sets, separately for symmetric and asymmetric ones (panels (a) and (b), respectively; recall P is the total power defined by Eq. (4)). The results are collected in this figure for $\alpha = 0.15$, $Q = 1$, and $R = 2.3438$, which adequately represents a generic case. A general trend is destabilization with the increase of the total power, but there are exceptions, such as families of symmetric sets of four and seven solitons in panel (a). Another general trend is the destabilization with the increase of the number of solitons in the sets: as mentioned above, symmetric and asymmetric complexes cannot be built of more than seven and three individual solitons, respectively.

It is worthy to note that the comparison of panels (a) and (b) in Fig. 10 demonstrates bistability in the present system, which we understand as coexistence of different stable patterns at equal values of their total powers. First, the interval of values of the total power in which the asymmetric single-soliton states are stable overlaps with the stability interval of the symmetric single-soliton modes. Second, the stability intervals for the asymmetric three-soliton sets and symmetric four-soliton ones nearly coincide too.

Lastly, additional numerical results, obtained by varying distance R of each peak from the center, demonstrate that all two and three-soliton sets, with each soliton pinned to a singularity peak, tend to become stable with the increase of R , for a simple reason that weak interactions between far separated solitons cannot conspicuously destabilize their bound states. In particular, the diagram for the asymmetric sets, displayed in Fig. 10(b), does not feature any stable two-soliton complexes at $R = 2.3438$, while at $R = 3.1250$ a stable two-soliton state is readily found, as shown in Fig. 8(b).

4 Vortex-soliton rings

Three-soliton sets carrying intrinsic vorticity were generated starting from the input built as a ring-shaped chain of three fundamental solitons attached to the singular-modulation peaks (A, B, C in Fig. 1), with phase shift $2\pi/3$ between

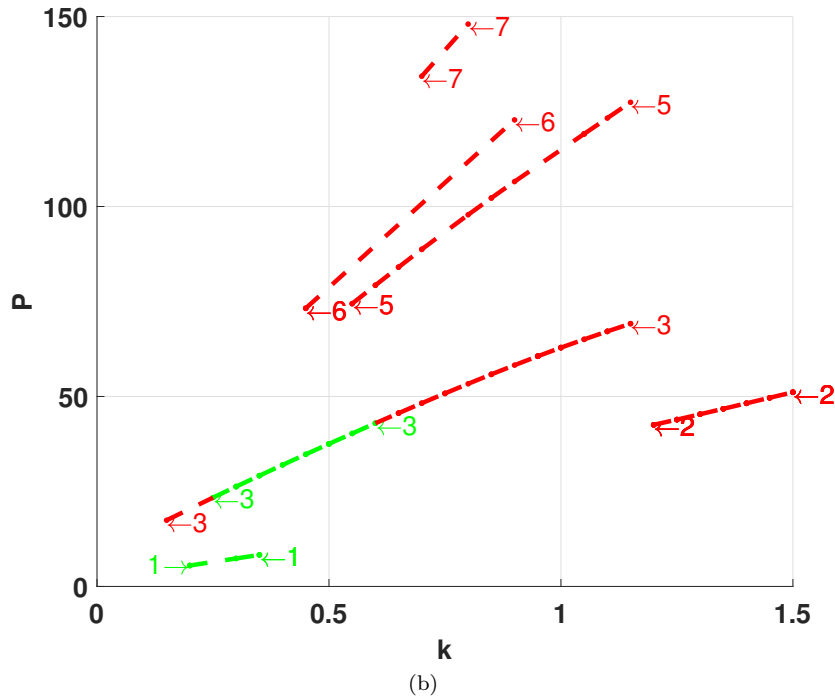
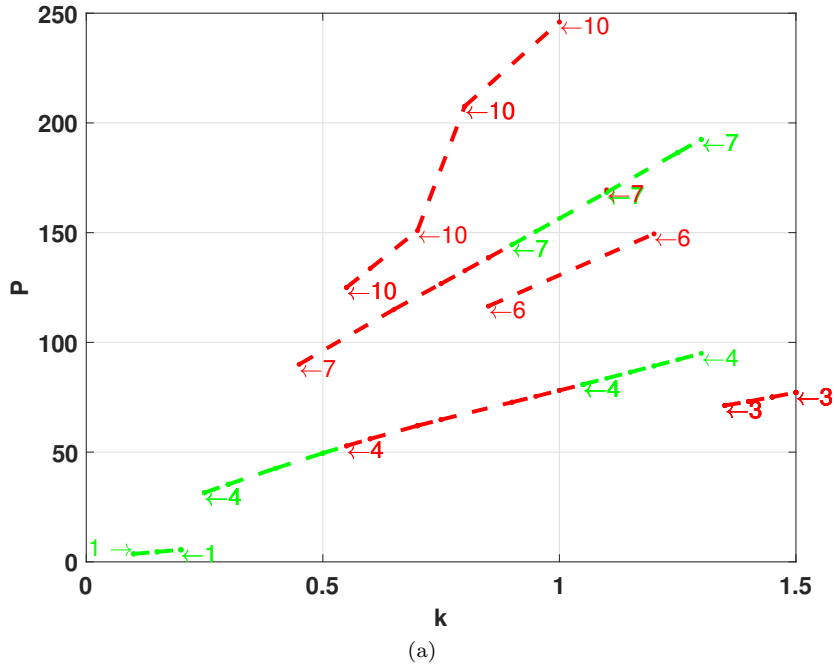


Figure 10: (Color online) Typical existence and stability maps for single- and multi-solitons states, shown in the plane of the propagation constant, k , and total power (P , see Eq. (4)), for $\alpha = 0.15, Q = 1$ and $R = 2.3438$. Numbers attached to edges of the $P(k)$ lines, and to their internal breakup points (see the top line in (a) labeled “10”) denote the number of individual solitons in the respective sets. Green and red colors of the lines and attached numbers designate stable and unstable sets, respectively. Panels (a) and (b) separately display the results for symmetric and asymmetric soliton complexes.

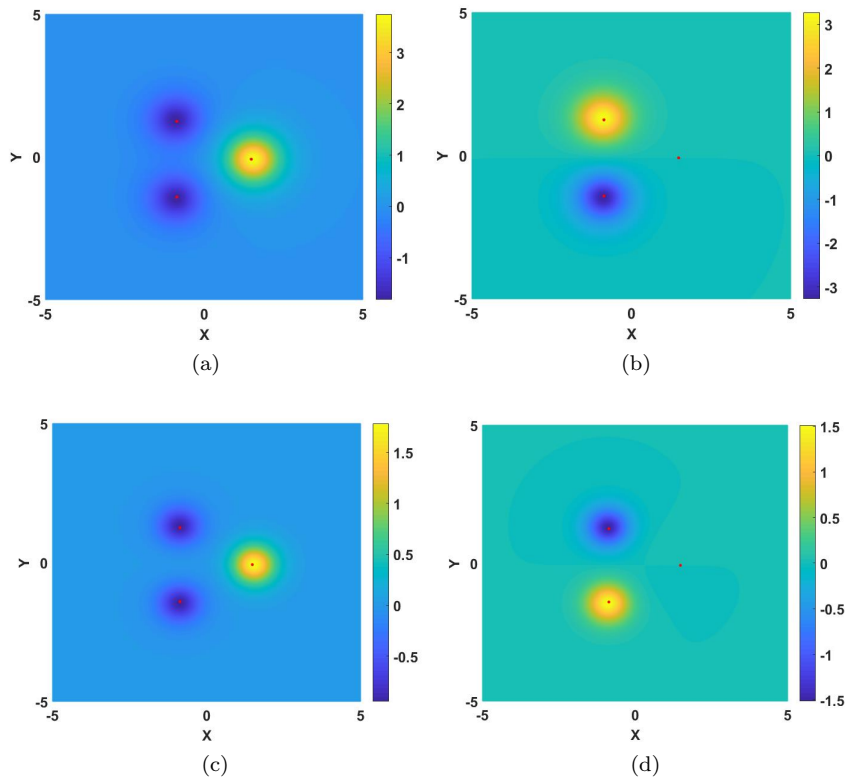


Figure 11: (Color online) A stable three-soliton ring with imprinted vorticity $S = 1$, for parameters $\alpha = 0.15, Q = 1, R = 1.5625$, and $k = 1.5$. Panels (a) and (b) display the real and imaginary parts of the FH field; (c) and (d): the same for the SH field.

FF components of adjacent solitons, which corresponds to the overall phase circulation of 2π in the FF field (and 4π in its SH counterpart), i.e., vorticity $S = 1$ *imprinted* onto the soliton ring:

$$\begin{aligned}\varphi(x, y) &= \varphi_A(x, y) + \varphi_B(x, y)e^{2\pi i/3} + \varphi_C(x, y)e^{4\pi i/3}, \\ \psi(x, y) &= \psi_A(x, y) + \psi_B(x, y)e^{4\pi i/3} + \psi_C(x, y)e^{8\pi i/3},\end{aligned}\quad (26)$$

where subscripts A, B, and C refer to standard fundamental-soliton solutions with their centers placed at the respective singular peaks (in the last term of the expression for ψ , $e^{8\pi i/3}$ is identical to $e^{2\pi i/3}$). An example of the so constructed stable vortex complex is displayed in Fig. 11.

As shown in Fig. 12, the stability of vortex rings essentially depends on size R of the three-peak configuration: as well as in case of zero-vorticity multisoliton sets (see above), the vortex rings tend to stabilize themselves with the increase of R , which is explained by weaker interaction between far separates solitons. The stability region in Fig. 12 somewhat expands with the increase of k , because this entails shrinkage of each individual soliton, making its relative size with

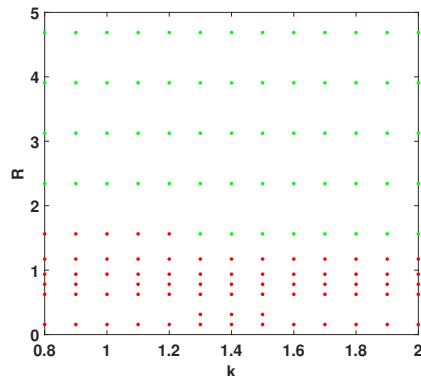


Figure 12: (Color online) The stability diagram for vortex-ring solitons at $Q = 1$ and $\alpha = 0.15$ in the plane of the propagation constant k and the distance of each singularity peak from the center, R . Green and red dots denote, respectively, stable and unstable vortices.

respect to R smaller, thus also effectively weakening the interaction between solitons.

Lastly, in direct simulations the vortex rings, which are predicted to be unstable in terms of eigenvalues of small perturbations, demonstrate spontaneous transformation into a single stable soliton, with a small “remnant” of another one, as shown in Fig. (13)

5 Conclusion

Using the recent result which demonstrates the existence of stable 2D solitons in the medium with the quadratic interaction supported by the local $\chi^{(2)}$ coefficient which is subject to the locally singular modulation, we have introduced the system with the equilateral triangle of three singular-modulation peaks. This system makes it possible to predict new 2D multi-soliton patterns, including ones symmetric and asymmetric with respect to the underlying triangular structure, and introduce vortex-ring patterns. The stability of the stationary solutions was identified through the computation of the respective perturbation eigenvalues, and verified by direct simulations. The asymmetric position of the single-soliton state, shifted off the system’s center, was accurately predicted analytically. Zero-vorticity (fundamental) multi-soliton sets were built with the number of solitons from 1 to 10. Symmetric sets constructed of 1, 4, and 7 solitons have their stability regions, while stable asymmetric patterns may contain 1, 2, or 3 solitons. Symmetric and asymmetric sets composed of 1 or 3 and 4 solitons feature mutual bistability. All sets elongated in a particular direction feature alternating signs of the fundamental-frequency components of constituent solitons in that direction. Unstable patterns spontaneously transform themselves into stable ones, with a smaller number of individual solitons in them. Vortex rings, composed of three solitons, are stable if interactions between individual solitons are sufficiently weak.

These results present a contribution to the vast topic of pattern formation in spatial-domain nonlinear optics [48]-[52]. As an extension of this work, it may

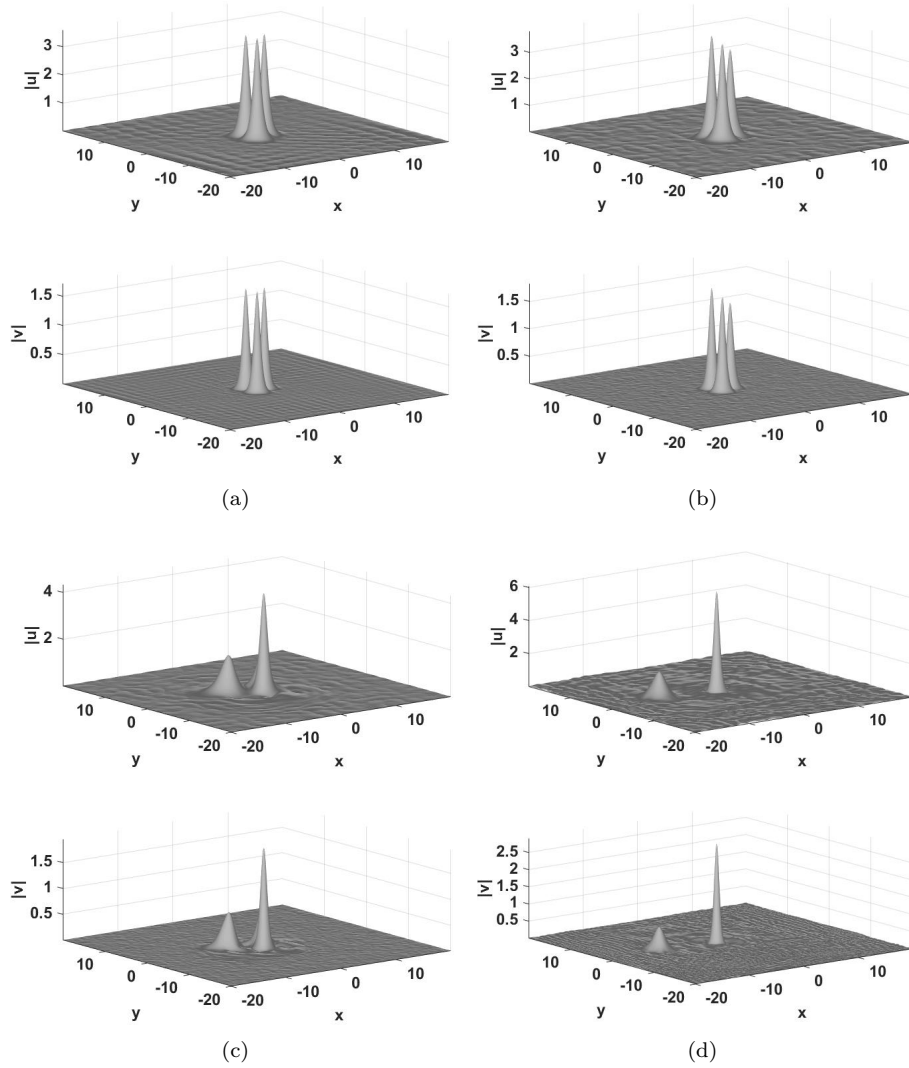


Figure 13: Unstable evolution of a vortex ring, originally built of three individual solitons, with $k = 1.1$. Other parameters are $Q = 1$, $\alpha = 0.15$, and $R = 1.5625$. Panels (a), (b), (c) and (d) display, respectively, the absolute value of the FF and SH fields at $z = 20, 60, 80$ and 100 .

be interesting to consider a system of three waves coupled by the singularly modulated quadratic Type-II interaction.

Acknowledgments

We thank Prof. C. L. P. Lambruschini for the invitation to submit a contribution to this Special Issue of EPJ - ST. This work was supported, in a part, by the Israel Science Foundation through grant No. 1287/17.

Authors' contributions

The work was designed by B.A.M., who was also responsible for the analytical part. V.L. has performed the numerical computations. Both authors equally contributed to drafting the paper.

References

- [1] Y. S. Kivshar, and G. P. Agrawal, *Optical Solitons: From Fibers to Photonic Crystals* (Academic Press, San Diego, 2003).
- [2] T. Dauxois and M. Peyrard, *Physics of Solitons* (Cambridge University Press: Cambridge, 2006).
- [3] W. A. Harrison, *Pseudopotentials in the Theory of Metals* (Benjamin: New York, 1966).
- [4] Y. V. Kartashov, B. A. Malomed, and L. Torner, *Rev. Mod. Phys.* **83**, 247 (2011).
- [5] L. P. Pitaevskii and A. Stringari, *Bose-Einstein Condensation* (Clarendon Press:, Oxford, 2003).
- [6] J. Hukriede, D. Runde, and D. Kip, *J. Phys. D* **36**, R1 (2003).
- [7] R. Yamazaki, S. Taie, S. Sugawa, and Y. Takahashi, *Phys. Rev. Lett.* **105**, 050405 (2010).
- [8] L. W. Clark, L.-C. Ha, C.-Y. Xu, and C. Chin, *Phys. Rev. Lett.* **115**, 155301 (2015).
- [9] S. Ghanbari, T. D. Kieu, A. Sidorov, and P. Hannaford, *J. Phys. B: At. Mol. Opt. Phys.* **39**, 847 (2006).
- [10] D. M. Bauer, M. Lettner, C. Vo, G. Rempe, and S. Dürr, *Nature Phys.* **5**, 339 (2009).
- [11] O. V. Borovkova, V. E. Lobanov, and B. A. Malomed, *Phys. Rev. A* **85**, 023845 (2012).
- [12] L. Bergé, *Phys. Rep.* **303**, 259 (1998).
- [13] G. Fibich, *The Nonlinear Schrödinger Equation: Singular Solutions and Optical Collapse* (Springer: Cham, 2015).
- [14] G. I. Stegeman, D. J. Hagan, and L. Torner, *Opt. Quant. Electr.* **28**, 1691 (1996).
- [15] C. Etrich, F. Lederer, B. A. Malomed, T. Peschel, and U. Peschel, *Progr. Optics* **41**, 483 (2000).
- [16] A. V. Buryak, P. Di Trapani, D. V. Skryabin, and S. Trillo, *Phys. Rep.* **370**, 63 (2002).
- [17] H. Suchowski, G. Porat, and A. Arie, *Laser Photonics Rev.* **8**, 333 (2014).
- [18] M. M. Fejer, G. A. Magel, D. H. Jundt, and R. L. Byer, *IEEE J. Quant. Electr.* **28**, 2631 (1992).
- [19] M. Yamada, N. Nada, M. Saitoh, and K. Watanabe, *Appl. Phys. Lett.* **62**, 435.
- [20] V. Berger, *Phys. Rev. Lett.* **81**, 4136(1998).

- [21] R. Lifshitz, A. Arie, and A. Bahabad, *Phys. Rev. Lett.* **95**, 133901 (2005).
- [22] A. Arie, N. Habshoosh, and A. Bahabad, *Opt. Quant. Electr.* **39**, 361 (2007).
- [23] A. Arie and N. Voloch, *Laser Phot. Rev.* **4**, 355 (2010).
- [24] A. A. Sukhorukov and Y. S. Kivshar, *Phys. Rev. E* **65**, 036609 (2002).
- [25] A. Shapira, N. Voloch-Bloch, B. A. Malomed, and A. Arie, *J. Opt. Soc. Am. B* **28**, 1481 (2011).
- [26] V. A. Brazhnyi and B. A. Malomed, *Phys. Rev. A* **86**, 013829 (2012).
- [27] V. Lutsky and B. A. Malomed, *Phys. Rev. A* **91**, 023815 (2015).
- [28] B. A. Malomed, editor: *Spontaneous Symmetry Breaking, Self-Trapping, and Josephson Oscillations* (Springer-Verlag: Berlin and Heidelberg, 2013).
- [29] S. Flach and V. Fleurov, *J. Phys. Cond. Matt.* **9**, 7039 (1997).
- [30] R. A. Pinto and S. Flach, *Phys. Rev. A* **73**, 022717 (2006).
- [31] T. Lahaye, T. Pfau, and L. Santos, *Phys. Rev. Lett.* **104**, 160404 (2010).
- [32] L. Li and P. G. Kevrekidis, *Phys. Rev. E* **83**, 066608 (2011).
- [33] J. D'Ambrose, P. G. Kevrekidis, and S. Lepri, *J. Phys. A Math. Theor.* **45**, 444012 (2012).
- [34] G. Gligorić, A. Radovanović, J. Petrović, A. Maluckov, Lj. Hadzievski, and B. A. Malomed, *Chaos* **27**, 113102 (2017).
- [35] R. Franzos and V. Penna, *Phys. Rev. E* **67**, 046227 (2003).
- [36] A. Sigler, B. A. Malomed, and D. V. Skryabin, *Phys. Rev. E* **74**, 066604 (2006).
- [37] P. Jason and M. Johansson, *Phys. Rev. E* **91**, 022910 (2015).
- [38] Z. Shen, L. Su, X.-C. Yuan, and Y.-C. Shen, *Appl. Phys. Lett.* **109**, 241901 (2016).
- [39] J. Yang, *Nonlinear Waves in Integrable and Nonintegrable Systems* (SIAM: Philadelphia, 2010).
- [40] D. E. Pelinovsky, *Localization in Periodic Potentials* (Cambridge University Press: Cambridge, 2011).
- [41] V. Lutsky and B. A. Malomed, *Opt. Exp.* **25**, 12967 (2017).
- [42] M. Vakhitov and A. Kolokolov, *Radiophys., Quantum Electron.* **16**, 783 (1973).
- [43] W. J. Firth and D. V. Skryabin, *Phys. Rev. Lett.* **79**, 2450 (1997).
- [44] L. Torner and D. V. Petrov, *Electron. Lett.* **33**, 608 (1997).

- [45] D. V. Petrov, L. Torner, J. Martorell, R. Vilaseca, J. P. Torres, and C. Cojocaru, *Opt. Lett.* **23**, 1444 (1998).
- [46] D. V. Skryabin and W. J. Firth, *Phys. Rev. E* **58**, R1252 (1998).
- [47] B. A. Malomed, *Phys. Rev. E* **58**, 7928 (1998).
- [48] N. N. Rosanov, *Progr. Opt.* **35**, 1-60 (1996).
- [49] F. T. Arecchi, S. Boccaletti, and P. Ramazza, *Phys. Rep.* **318**, 1 (1999).
- [50] B. Gutlich, H. Zimmermann, C. Denz, R. Neubecker, M. Kreuzer, T. Tschudi, *Appl. Phys. B: Laser Opt.* **81**, 927 (2005).
- [51] T. Ackemann, W. J. Firth, and G.-L. Oppo, *Adv. At. Mol. Opt. Phys.* **57**, 323 (2009).
- [52] A. S. Reyna and C. B. de Araujo, *Adv. Opt. Phot.* **9**, 720 (2017).